



Protective effects and regulatory mechanisms of Shen-shuai-yi recipe on renal fibrosis in unilateral ureteral obstruction-induced mice

Ping-lan Lin^{a,b,1}, Tao-tao Weng^{a,b,1}, Lian-xiang Duan^a, Lin-zhang Zhang^b, Xia Wei^b, Sheng-lan Qi^b, Jia-wen You^c, Yu Cao^a, Guang-bo Ge^d, Wei Liu^{b,*}, Xiao-li He^{c,**}, Jing Hu^{a,***}

^a Department of Nephropathy, The Seventh People's Hospital, Shanghai University of Traditional Chinese Medicine, Shanghai, China

^b Key Laboratory of Liver and Kidney Diseases (Ministry of Education), Department of Pharmacy, Institute of Kidney Disease, Shanghai Key Laboratory of Traditional Chinese Clinical Medicine, Shuguang Hospital Affiliated to Shanghai University of Traditional Chinese Medicine, Shanghai, China

^c Department of Endocrinology, Yueyang Hospital of Integrated Traditional Chinese and Western Medicine, Shanghai University of Traditional Chinese Medicine, Shanghai, China

^d Shanghai Frontiers Science Center of TCM Chemical Biology, Institute of Interdisciplinary Integrative Medicine Research, Shanghai University of Traditional Chinese Medicine, Shanghai, China

ARTICLE INFO

Keywords:

Renal fibrosis
Chronic kidney disease
Ureteral unilateral obstruction
Shen-shuai-yi recipe
Signal transducer and activator of transcription 3

ABSTRACT

Renal fibrosis (RF) is a common pathological feature of chronic kidney disease (CKD), which remains a major public health problem. As now, there is still lack of chemical or biological drugs to reverse RF. Shen-shuai-yi Recipe (SSYR) is a classical Chinese herbal formula for the treatment of CKD. However, the effects and mechanisms of SSYR in treating RF are still not clear. In this study, the active constituents SSYR for treating RF were explored by UHPLC-Q-Orbitrap HRMS. Bioinformatics analyses were employed to analyze the key pharmacological targets and the core active constituents of SSYR in the treatment of RF. In experimental validation, vehicle or SSYR at doses of 2.12 g/kg/d and 4.25 g/kg/d were given by orally to unilateral ureteric obstruction (UUO) mice. 13 days after treatment, we detected the severity of renal fibrosis, extracellular collagen deposition and pre-fibrotic signaling pathways. Bioinformatics analysis suggested that signal transducer and activator of transcription 3 (STAT3) was the core target and lenticin, luteolin-7-O-rutinoside, hesperidin, kaempferol-3-O-rutinoside, and 3,5,6,7,8,3',4'-heptamethoxyflavone were the key constituents in SSYR for treating RF. SSYR significantly reduced the expressions of fibronectin (FN), α -smooth muscle actin (α -SMA), collagen-I and alleviated renal interstitial collagen deposition in UUO kidneys. In mechanism, SSYR potently blocked the phosphorylation of STAT3 and Smad3 and suppressed the expression of connective tissue growth factor (CTGF). Collectively, SSYR can ameliorate RF via inhibiting the phosphorylation of STAT3

* Corresponding author.

** Corresponding author.

*** Corresponding author.

E-mail addresses: lwhzayl@163.com (W. Liu), fishstata@163.com (X.-l. He), 6264570@qq.com (J. Hu).

¹ These authors have contributed equally to this work.

<https://doi.org/10.1016/j.heliyon.2023.e17908>

Received 5 February 2023; Received in revised form 29 June 2023; Accepted 30 June 2023

2405-8440/© 2023 The Authors. Published by Elsevier Ltd. This is an open access article under the CC BY-NC-ND license (<http://creativecommons.org/licenses/by-nc-nd/4.0/>).

and its downstream and reducing the collagen deposition, suggesting that SSYR can be developed as a novel medicine for treating RF.

1. Introduction

Chronic kidney disease (CKD) is a leading public health problem worldwide with a global estimated prevalence of 13.4% [1]. Renal fibrosis (RF) is a common pathological feature of CKD which characterized by excessive deposition of extracellular matrix (ECM) proteins and activation of pro-fibrotic signaling pathways, which accelerates the decline of renal function and the destruction of renal structure [2]. Despite the seriousness of this problem, there is not enough clinical treatment for RF. Therefore, the key scientific problem of current research is to find more effective therapies to treat RF and reduce medical expenditure [3].

Traditional Chinese medicines (TCMs) are used as an alternative therapy for the treatment of CKD as its advantages in protecting renal function, delaying the process of renal fibrosis [4], and furtherly improving the quality of life and long-term survival of patients [5]. Shen-shuai-yi Recipe is an empirical prescription to treat CKD fibrosis since the 1980s [6]. Clinical studies illustrated that SSYR obviously improves renal function via down regulation of inflammation and oxidative stress [7]. However, the effects and mechanisms of SSYR in treating RF is still not clear.

In this study, the active constituents and mechanisms of SSYR for treating RF were explored by integrating Ultra high performance liquid chromatography Q exactive hybrid quadrupole orbitrap high resolution accurate mass spectrometry (UHPLC-Q-Orbitrap HRMS), bioinformatics analysis and experimental pharmacology. This study might be providing scientific evidence of SSYR on RF and will be helpful in developing potential drug candidates in the future.

2. Materials and methods

2.1. Drugs and reagents

Hematoxylin and Eosin (H&E) staining kit (D006-1-1), and Masson's trichrome staining kit (D026-1-3) were purchased from Nanjing Jiancheng Bioengineering Institute (Nanjing, China). Sirius Red staining kit (G1472) was purchased from Solarbio Science & Technology Co., Ltd. (Beijing, China), Losartan tablets (100 mg/tablet) were obtained from MSD Pharmaceutical Co., Ltd. (Hangzhou, China) and used as a positive control [8]. Aloe-emodin, rhein, emodin, chrysophanol and physcion were purchased from Dalian Meilun Biotechnology Co., Ltd. (Dalian, China). Aloe-emodin-8-O-b-D-glucopyranoside, rhein-8-O-b-D-glucopyranoside, emodin-1-O-glucoside, emodin-8-glucoside, chrysophanol-8-O-b-D-glucopyranoside and chrysophanol-1-O-b-D-glucopyranoside were purchased from Chengdu Biopurify Phytochemicals Ltd. (Chengdu, China). Composition of SSYR was presented in Table 1. The herbs in SSYR were purchased from Kangqiao Chinese Medicine Tablet Co., Ltd (Shanghai, China).

2.2. Animals

SPF-grade male C57BL/6 mice (weighing 20 ± 2 g) aged 6 weeks were acquired from Shanghai SLAC Laboratory Animal Co., Ltd. and kept in the Shanghai University of Traditional Chinese Medicine's animal center. The animals were kept in a temperature-controlled breeding chamber, where the temperature was set to 25 °C and the day-night cycle was 12 h. All animal protocols were approved by Committee on the Ethics of Animal Experiments of SHUTCM (Approval Number: PZSHUTCM220711030 and PZSHUTCM220711031).

2.3. Preparation of the Chinese multi-herbal formula Shen-shuai-yi recipe (SSYR)

According to the composition of the Shen-shuai-yi Recipe (SSYR), 480 g herbs (including 30 g *Rheum palmatum* L., 90 g *Smilax glabra* Roxb., 90 g *Vaccaria segetalis* (Neck. Garcke.), 30 g *Citrus reticulata* Blanco., 30 g *Angelica sinensis* (Oliv.) Diels., 30 g *Pinellia ternata* (Thunb.), 90 g *Astragalus membranaceus* (Fisch.) Bge. var. *mongholicus* (Bge.) Hsiao and 90 g *Trigonella foenum-graecum* L. were mixed together. 2.4 L deionized water were added, and mixed herbs were macerated for 30 min. After then, the mixed herbs were

Table 1
Composition of Shen-shuai-yi recipe.

Chinese name	Botanical name	English name	Parts used	Proportion (g)
Dang gui	<i>Angelica sinensis</i> (Oliv.) Diels	Angelicae Sinensis Radix	Root	10
Huang qi	<i>Astragalus membranaceus</i> (Fisch.) Bge. var. <i>mongholicus</i> (Bge.) Hsiao	Astragali Radix	Root	30
Ban xia	<i>Pinellia ternata</i> (Thunb.)	Pinelliae Rhizoma	Rhizome	10
Chen pi	<i>Citrus reticulata</i> Blanco	Citri Reticulatae Pericarpium	Peel	10
Tu fu ling	<i>Smilax glabra</i> Roxb.	Smilacis Glabrae Rhizoma	Rhizome	30
Wang bu liu xing	<i>Vaccaria segetalis</i> (Neck.) Garcke	Vaccariae Semen	Seed	30
Hu lu ba	<i>Trigonella foenum-graecum</i> L.	Trigonellae Semen	Seed	30
Da huang	<i>Rheum palmatum</i> L.	Rhei Radix et Rhizoma	Root and rhizome	10

decocted for 45 min by 2.4 L water twice. The twice extracted liquid was filtered and merged. The extracted liquid was subsequently concentrated by rotary evaporation under reduced pressure, and the concentrated extract was vacuum dehydrated, and then the extract of SSYR was successfully prepared (74.2 g, extract yield was 15.46% from SSYR). 1.0 g SSYD was weighed, it was dissolved in 50 mL deionized water under ultrasonic for 1 h, and then, the solution was centrifuged (10 000×g for 15 min). The supernatant solution was filtered by 0.22 µm membrane, and the filtered solution was used for chemical analysis.

2.4. Chemical profiling of SSYR by UHPLC-Q-Orbitrap HRMS

The chemical profiling of SSYR was analyzed by using UHPLC-Q-Orbitrap HRMS (Thermo Fisher Scientific Inc., Grand Island, NY, USA). The UHPLC was Dionex Ultimate 3000, and it was controlled by Chromeleon (version 7.2). The column heater was set at 45 °C and the cooling autosampler was set at 10 °C. An UPLC BEH C₁₈ column (2.1 × 100 mm, 1.7 µm, Waters) was employed. The mobile phase consisted of 0.1% formic acid water (A) and methanol (B). The flow rate was set at 0.3 mL/min, while the following gradient elution was used: 0–2.0 min, 4% B; 2.0–6.0 min, 4–12% B; 6.0–38.0 min, 12–70% B; 38.0–38.5 min, 70% B; 38.5–39.0 min, 70–95% B; 39.0–43.0 min, 95% B; 43.0–45.0 min, 4% B. Subsequently, the extract of SSYR (2 µL) was injected into the UHPLC-Q-Orbitrap HRMS system equipped with an electrospray ionization source, while Xcalibur (version 4.1) was used for data recording and data analysis. The electrospray ionization source was operated in positive and negative ionization mode. The parameters of mass spectrometry were optimized and listed below: capillary temperature set at 320 °C; sheath gas (N₂) flow rate set at 35 arbitrary units; auxiliary gas (N₂) flow rate set at 10 arbitrary units; sweep gas flow rate set at 0 arbitrary units; spray voltage set at 2.8 kV (negative) and 3.5 kV (positive); S-lens RF level set at 50 V; auxiliary gas heater temperature set at 300 °C; scan mode was used Full MS/SIM and Full MS/dd-MS2 mode. The Full MS/dd-MS2 mode includes 1 full scan (resolution set at 70000 FWHM) and 1 data-dependent secondary scan (resolution set at 17500 FWHM) 2 events, the scanning range is 80–1200 *m/z*, and the gradient of collision energy is set at 10, 20, 40 V.

2.5. Target genes prediction of renal fibrosis

GeneCards (<https://www.genecards.org>), Therapeutic Target Database (TTD, <https://db.idrblab.org/ttd/>), OMIM (<https://omim.org>), and MalaCards (<http://www.malacards.org/>) database were used to search for disease-related target genes using the terms 'renal fibrosis'.

2.6. Identification of the components and the prediction targets of SSYR in treating renal fibrosis

The components of SSYR were identified by UHPLC-Q-TOF-MS analysis. We obtained the treatment targets of SSYR by importing the SMILES strings of the active components into Swiss Target Prediction (<http://www.swisstargetprediction.ch/>) tool. The targets with "Probability >0" were regarded as the potential therapeutic targets. We downloaded every structure file corresponding to the active ingredients from Durgbank (<https://go.drugbank.com/>) and Pubchem (<https://pubchem.ncbi.nlm.nih.gov/>) database. The names of potential therapeutic targets were collected from Uniprot (<https://www.uniprot.org/>) and Genecards database. The Venn diagram was created by an online Venn tool (<http://bioinformatics.psb.ugent.be/webtools/Venn/>).

2.7. Bioinformatics analysis and screening of core therapeutic targets of SSYR

The intersecting targets on Venn diagram obtained between the potential therapeutic targets of SSYR and the pathological genes of renal fibrosis were considered as the key treatment target hub, R&S. The protein-protein interaction (PPI) network of R&S was established by the STRING database. We downloaded the network and imported it into Cytoscape (version 3.6.1) software for further topological analysis. The core therapeutic targets of SSYR were determined by topological analysis. Gene Ontology (GO) enrichment evaluated biological process, molecular function and cellular component of R&S. GO analysis was performed by the R software.

2.8. Virtual molecular docking

The active components of SSYR were collected from the UHPLC-Q-TOF-MS analysis. The 2D structures of the constituents were downloaded from the RCSB PDB database (<https://www.pdbus.org/>). The PDB files of the R&S core targets were obtained from the RCSB PDB database (<https://www.pdbus.org/>). We used PyMOL software (version for education 2.2.0) to preprocess the protein structure by deleting the H₂O and some small molecules, adjusting hydrogen atoms, and defining the right bond orders. After correcting the structure defects, we minimized the energy of the protein. The 2D structures in mol2 format were imported into the AutoDock Vina software (version 1.2.0) and transformed into pdbqt format files. We used AutoDock Vina to conduct semi-flexible dockings of the active components with the target protein into the catalytic active domain. The molecular docking scores were calculated and the 3D diagram of the interaction between the receptor and the ligand was plotted.

2.9. Characterization of the absorbed chemical constituents in mice serum and kidney after oral administration of SSYR

After seven days of acclimatization, the mice (n = 6, male) were randomly divided into two groups. SSYR group (n = 3) was administered SSYR by gavage (4.25 g dried extract/kg, extrapolated from human equivalent dose), control group (n = 3) was

administered equal volume deionized water by gavage. Before the experiments, all mice were fasted overnight, and it had free access to water. And then, all mice were anaesthetized after the once oral administration at 1 h. Blood samples were collected from the abdominal aorta. Then, serum samples were obtained by centrifuged (5000×g, 15 min, 4 °C). All samples were stored at ultra-low temperature freezer (−80 °C) until analysis. The 200 μL of serum samples were added 1 mL methanol, vortexed and centrifuged (10 000×g, 15 min). The supernatant (960 μL) was dried by using N₂. The residue was redissolved in 80 μL 20% methanol, vortexed and centrifuged (10 000×g, 15 min), and the supernatant solution was used as the LC/MS sample. The 100 mg kidney tissue is homogenized in methanol (1 mL), the homogenate of them is centrifuged (10 000×g, 15 min, 4 °C). The supernatant (800 μL) is dried by using N₂. The residue is redissolved in 20% methanol (160 μL), vortexed and centrifuged (10 000×g, 15 min). The supernatant (2 μL) was analysis by UHPLC-Q-Orbitrap HRMS.

2.10. Intervention effects of SSYR on unilateral ureteral obstruction-induced renal interstitial fibrosis mouse model

For unilateral ureteral obstruction (UUO) mouse model, 8-week-old mice were anaesthetized with sodium pentobarbital (SP) (8 mg/kg, i.p.), and then a left flank incision was made to expose the left ureter which was ligated with 4–0 silk sutures [9]. The same operation was performed in sham mice except the ligation of ureter. Thirty-five mice were randomly divided into five groups: sham + Vehicle (saline) group (n = 7), UUO + Vehicle (saline) group (n = 7), sham + SSYR low-dose (2.12 g/kg) group (n = 7), UUO + SSYR high-dose (4.25 g/kg) group (n = 7) and UUO + Losartan (8.57 mg/kg) group (n = 7). Mice were treated with saline or daily by gavage for 13 days from the second day after surgery. Two weeks after the operation, mice were euthanized with SP (8 mg/kg, i.p.) and kidney tissues were collected for histopathological examination and Western blot.

2.11. Histological analysis

Kidneys were fixed in 4% paraformaldehyde and embedded with paraffin. Four-mm-thick tissue sections were performed for hematoxylin-eosin, Masson's trichrome (Masson), and Sirius Red staining according to the protocol. Positive staining was obtained and semi-quantitatively analyzed by Leica SCN400 Slide Scanning System and software (Leica, Inc., Wetzlar, GER). The severity of the renal injury was assessed by Paller's scoring method [10].

2.12. Western blotting analysis

Protein extraction and Western blot analysis were performed using previously described methods [11]. The band densities were measured using Quantity One software (Bio-Rad, USA). The primary and secondary antibodies are listed in [Supplementary Table S2](#).

2.13. Statistical analysis

All data were presented as means ± standard deviation (SD). One-way analysis of variance (ANOVA) with was used for the comparisons of differences among multiple groups and a *t*-test was used to compare the differences between two groups. When the *P* value < 0.05 the differences were considered statistically significant.

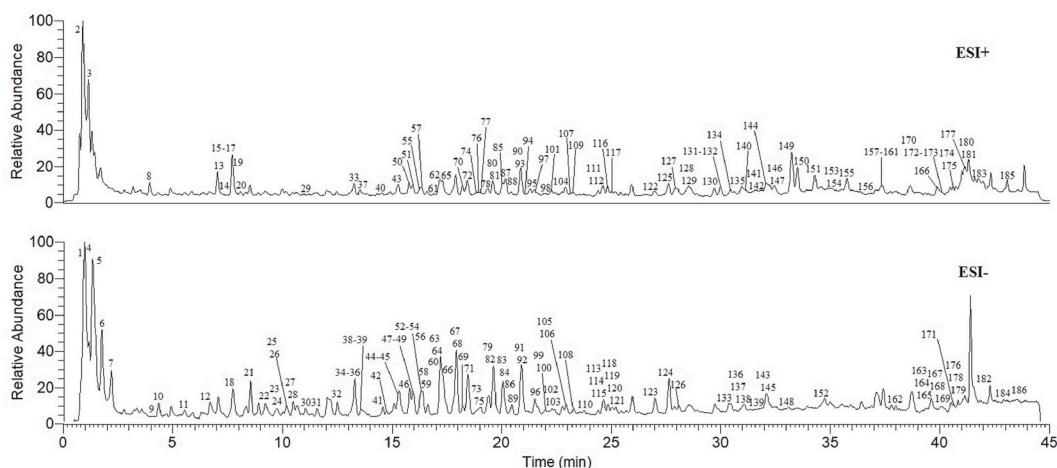


Fig. 1. The total ion chromatography of the extract of SSYR in positive (ESI+) and negative (ESI−) ion mode by UHPLC-Q-Orbitrap HRMS.

3. Results

3.1. Identification of the chemical constituents in extract and the absorbed constituents in mice serum and kidney after oral administration of SSYR

The identification of the chemical components in SSYR was completed by UHPLC-Q-Orbitrap HRMS. The total ion chromatograms (TICs) of the SSYR were showed in Fig. 1. The limit of errors of the protonated molecular weights of all identified compounds were set at within 10 ppm. After comparison with the MS/MS profiles and retention times of chemical standards, references and chemistry books, 186 chemical constituents were identified or tentatively determined from the SSYR. The detailed information (including retention times, precise molecular weights, error, molecular formula et al.) of identified chemical components in the SSYR were listed in Supplementary Table S1. The serum and kidney samples were collected from SSYR-treated mice at 1 h. And these samples were analysis by using UHPLC-Q-Orbitrap HRMS, which was detected the absorbed prototypes as more as possible. With the help of the key information of the identification chemical constituents in SSYR, a total of 70 and 45 prototype compounds were determined in serum and kidney, respectively.

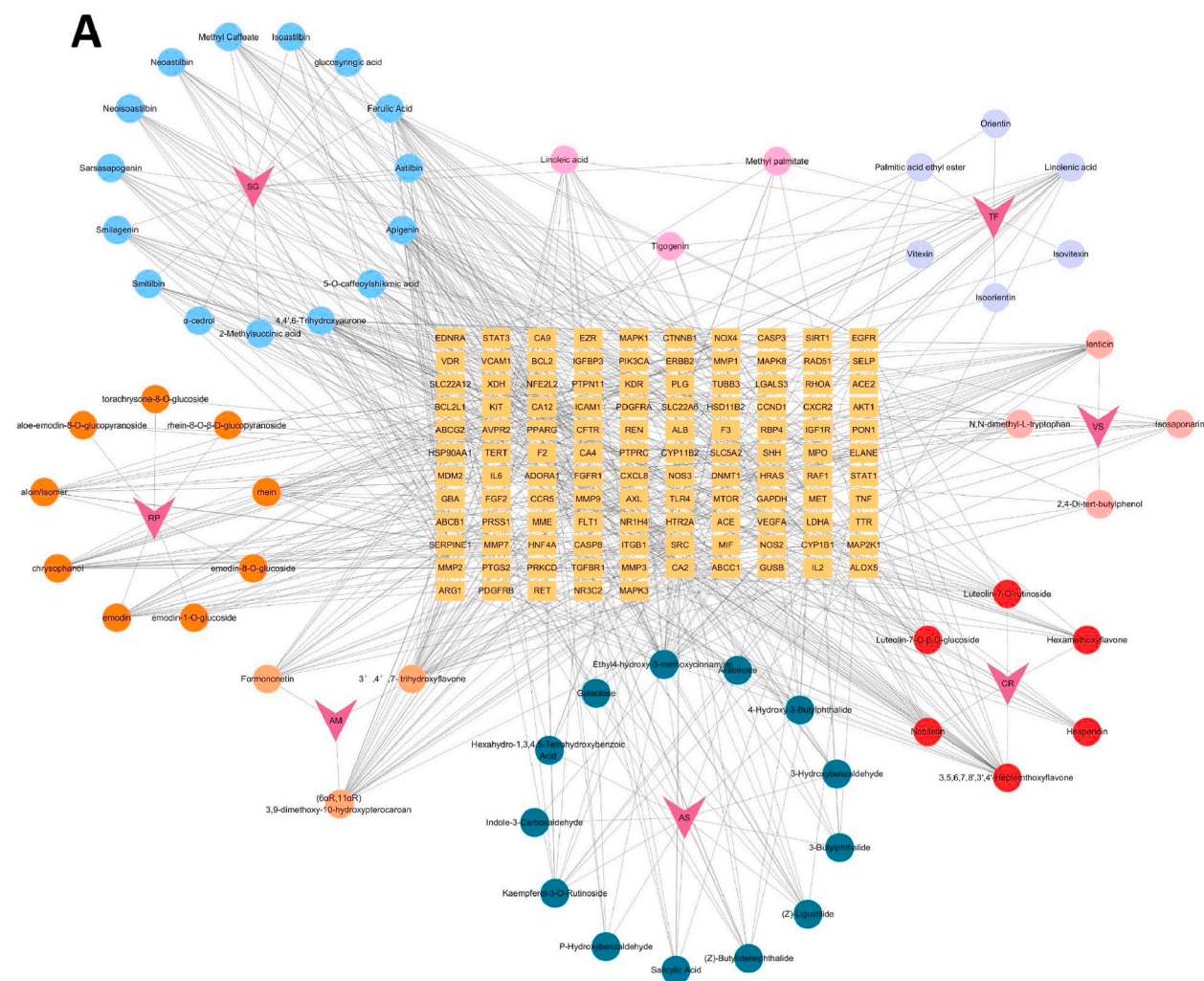


Fig. 2. The network analysis of the relationship between herb, components, and targets from SSYR. The herbs which have the top 3 numbers of active components are SG, AS, and RP. Linoleic acid, tigogenin, and methyl palmitate are the active components in common in SG and TF. The inverted triangles represent the herbs from SSYR. The circles represent the active components of each herb. The rectangles represent the potential targets that interacted with the active components. SG: *Smilax glabra* Roxb. AM: *Astragalus membranaceus* (Fisch.) Bge. var. *mongholicus* (Bge.) Hsiao. VS: *Vaccaria segetalis* (Neck.) Garcke. TF: *Trigonella foenum-graecum* L. RP: *Rheum palmatum* L. CR: *Citrus reticulata* Blanco. AS: *Angelica sinensis* (Oliv.) Diels.

3.2. The network pharmacological analysis and bioinformatic analysis of SSYR in the treatment of RF

An herb-molecular-target network was established to give a general description (Fig. 2A). It was noticed that the main active components belonged to *Smilacis Glabrae Rhizoma*, *Angelicae Sinensis Radix*, and *Rhei Radix et Rhizoma*. Linoleic acid, tigogenin, and methyl palmitate were the active components in common in *Smilacis Glabrae Rhizoma* and *Trigonellae Semen*. We collected 641 predicted targets of SSYR in treating renal fibrosis according to the method described forward. 1037 key genes in the occurrence and development of RF were downloaded from open-source databases. Then, the core gene hub (R&S) which contained 115 core genes was obtained by intersecting the predicted targets of SSYR and the key genes in RF (Fig. 3A).

Then, a systematic bioinformatic analysis was employed to analyze the potential target in the R&S. The topological analysis of the PPI network of R&S showed that STAT3, SRC, protein tyrosine phosphatase non receptor type 11 (PTPN11), heat shock protein 90AA1 (HSP90AA1), and mitogen-activated protein kinase 3 (MAPK3) were the top 5 core targets of SSYR in treating RF (Fig. 3B). The gene function analysis of R&S showed that STAT3, SRC, and PTPN11 had more comprehensive gene functions than other core genes (Fig. 3C and Supplementary Fig. S1). Through the topological analysis of the molecular-target interaction, the top component was apigenin which was a common flavonoid in plant herbs (Fig. 3D). Then, the GO enrichment analysis of R&S was operated. The genes of

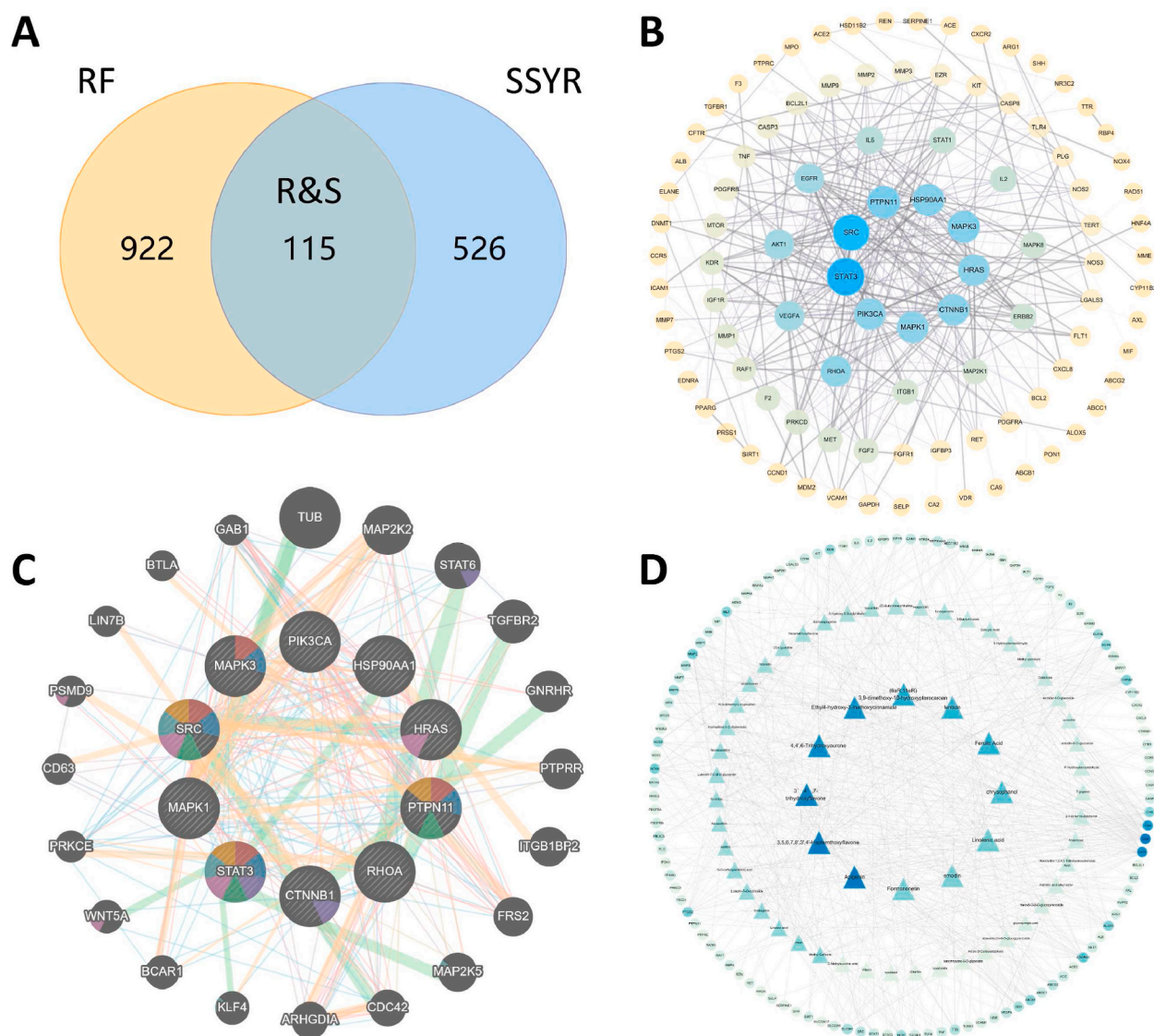


Fig. 3. The network pharmacological analysis of SSYR. (A) The core gene hub (R&S) is intersected by the key disease genes (RF) and the potential targets of SSYR (SSYR). (B) The topological analysis of the protein and protein interaction network. The larger size and the darker color of the circles represent the more important genes in the R&S. (C) The gene functions of the core genes (R&S). (D) The topological analysis of the active components and potential targets network. The triangles represent the active components from SSYR. The circles represent the potential targets. (For interpretation of the references to color in this figure legend, the reader is referred to the Web version of this article.)

R&S were enriched in biological process (Fig. 4A). The top 2 and 3 enriched biological processes were peptidyl-tyrosine modification and phosphorylation which were also indicated in gene function analysis (Fig. 4B). Tyrosine phosphorylation and modification were closely related to the phosphorylation of STAT3 as its crucial phosphorylation site was tyrosine amino acid residue 705. The cellular component analysis of R&S indicated that the main subcellular organelles participated were membrane microdomain, raft, and region (Fig. 4C). The top 3 enriched molecular functions of R&S were transmembrane receptor protein tyrosine kinase activity, transmembrane receptor protein kinase activity, and protein tyrosine kinase activity which were essential in the phosphorylation process of STAT3 (Fig. 4D). These analyses indicated that the interference of the activation of STAT3 may be a core link of SSSYR in the treatment of RF.

3.3. Virtual simulation of the constituents from SSSYR docking with STAT3

To further verify the key components and potential treatment targets, we employed virtual molecular docking and evaluated all the active components of SSSYR docking with STAT3 (PDB ID: 6NJS). The top 10 components sorted by binding energy in descending order were listed in Table 2. The top 5 components were lenticin, luteolin-7-O-rutinoside, hesperidin, kaempferol-3-O-rutinoside, and 3,5,6,7,8,3',4'-heptamethoxyflavone with -8.75 , -6.84 , -6.72 , -6.39 , and -6.04 kcal/mol, respectively. The 3D and 2D diagrams of each compound docking with the SH2 domain of STAT3 were presented in Fig. 5A–E. The SH2 domain was an amino acid strain from 584 to 688 which formed a highly conserved and key active pocket in STAT3. The inhibition of SH2 domain blocked the formation of STAT3-dimer which finally performed the catalytic activity. It was noticed that lenticin and linolenic acid could bind with the Ser613 and Glu612 sites while other components bound with the Glu638 site.

Despite lenticin, other components showed a mild binding performance with STAT3. Therefore, we evaluated lenticin and a potent STAT3 inhibitor SI109 ($IC_{50} = 3$ nM, as a positive control) docking with the SH2 domain of STAT3. As the results showed, lenticin, which was the main constituent of Vaccariae Semen, docked well into the catalytic pocket of STAT3. It bound to the Ser613, Ser611, and Glu612 sites with hydrogen bonds and the Glu638 site with H- π bond (Fig. 6A). The amino acid residues from 609 to 620 of SH domain was the key active sub-domain called pY pocket which strongly determined the phosphorylation of T705. Lenticin might be able to strongly bind to the pY pocket and inhibit the phosphorylation of STAT3. In addition, the binding sites of lenticin and the

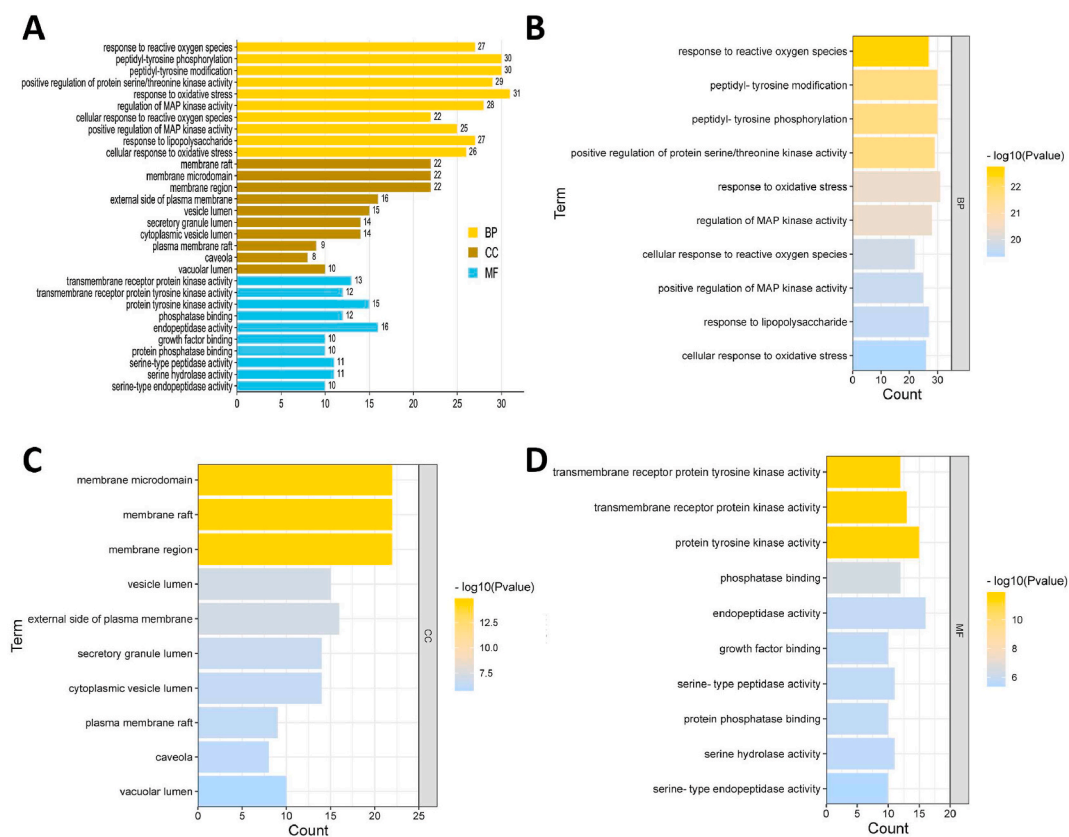


Fig. 4. The GO enrichment analysis of R&S. (A) The total histogram of GO enrichment analysis of R&S. (B) The biological process of GO enrichment analysis of R&S. (C) The cellular component of GO enrichment analysis of R&S. (D) The molecular function of GO enrichment analysis of R&S.

Table 2
The binding energy of the constituents of SSYR docking with the SH2 domain of STAT3.

Molecular	Binding energy (kcal/mol)
Lenticin	−8.75
Luteolin-7-O-rutinoside	−6.84
Hesperidin	−6.72
Kaempferol-3-O-rutinoside	−6.39
3,5,6,7,8,3',4'-Heptemthoxyflavone	−6.04
5-O-Caffeoylshikimic acid	−6.04
Hexamethoxyflavone	−6.00

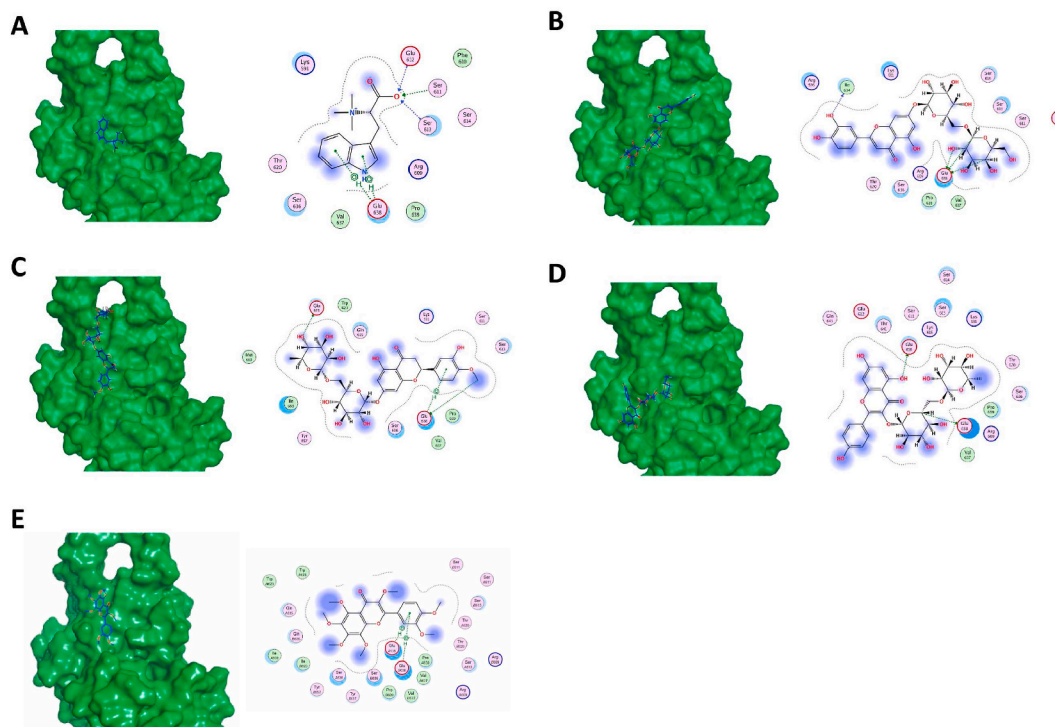


Fig. 5. The virtual simulation of the active components docking with STAT3. The molecular docking of the components from SSYR and STAT3 (PDB ID: 6NJS) with top 5 docking score. (A) Lenticin. (B) Luteolin-7-O-rutinoside. (C) Hesperidin. (D) Kaempferol-3-O-rutinoside. (E) 3,5,6,7,8,3',4'-Heptamethoxyflavone. The 3D illustrations of the top 5 components (lenticin, luteolin-7-O-rutinoside, hesperidin, kaempferol-3-O-rutinoside, and 3,5,6,7,8,3',4'-heptamethoxy-flavone) docking with the protein crystal of STAT3 (Left pictures). The 2D diagrams of the top 5 components docking with STAT3 (Right pictures).

positive control SI109 were very similar, especially in pY pocket (docking score: −8.75 versus −11.18 kcal/mol) (Fig. 6A and B). All the evidence above strongly indicates that SSYR may have a good effect on inhibiting the phosphorylation of STAT3 to treat RF and the key component is lenticin.

3.4. SSYR ameliorated tubulointerstitial fibrosis

UUO induced mouse model was used to validate the therapeutic efficacy of SSYR against renal injury and tubulointerstitial fibrosis. Firstly, the kidney of UUO mice exhibited severe structural damage, a decreased number and obvious expansion of tubules, widened tubulointerstitium and infiltration of inflammatory cells marked by H&E staining (Fig. 7D). We found that after treatment with 2.12 g/kg and 4.25 g/kg SSYR ($p < 0.01$; $p < 0.01$) improved the Paller's tubular injury score of UUO kidneys. Secondary, Masson's trichrome and Sirius Red staining revealed increased extracellular matrix and interstitial collagen deposition in UUO kidneys (Fig. 7A). The semi-quantitatively analyzed Masson's trichrome (Fig. 7B) and Sirius Red positive area (Fig. 7C) in kidney tissue decreased in two doses of SSYR treatment group ($p < 0.01$; $p < 0.01$). Furthermore, the protein expression of FN, α -SMA, Collagen-I were up-regulated in the kidneys of UUO mice (Fig. 8A), and high dose of SSYR treatment markedly reduced the expression of fibrosis-associated hallmarks ($p < 0.01$; $p < 0.01$; $p < 0.01$). In addition, the protein levels of p-Smad3 ($p < 0.01$; $p < 0.01$) and CTGF ($p < 0.01$; $p < 0.01$) were

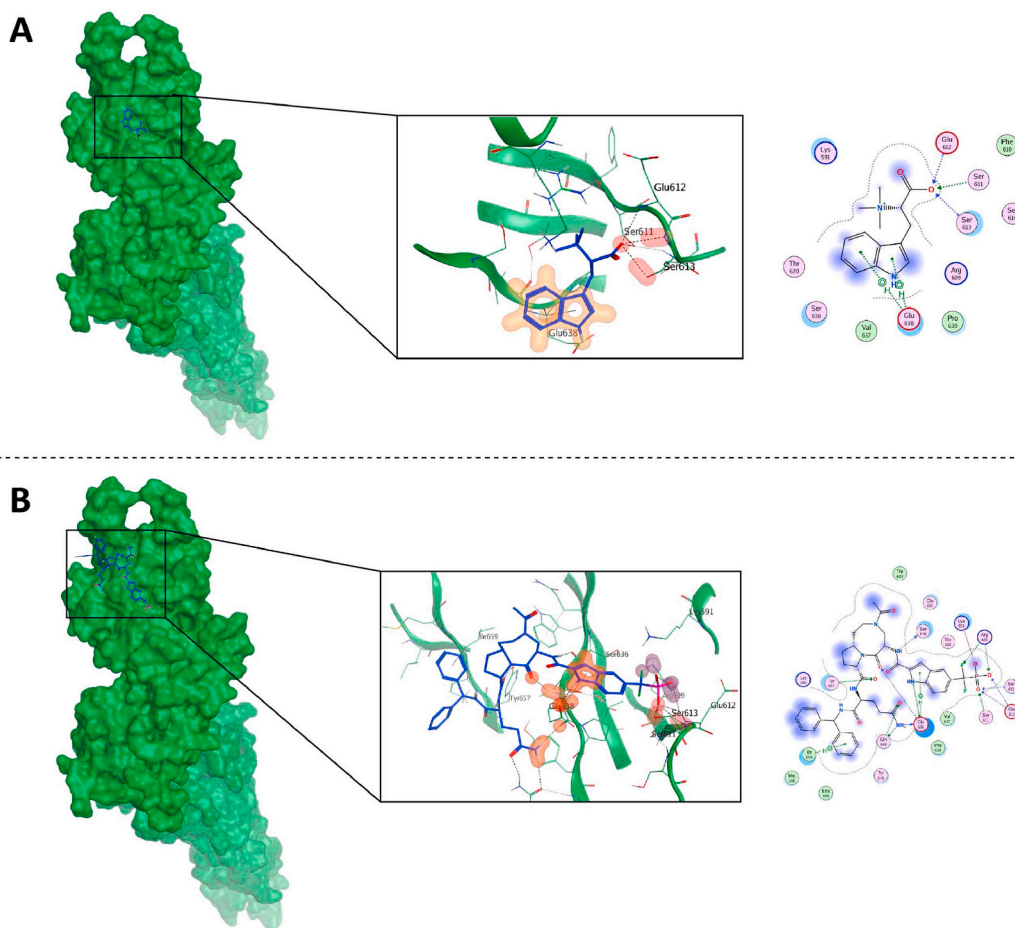


Fig. 6. The virtual simulation of lenticin and SI109 docking with STAT3. (A) The illustration of lenticin docking with STAT3. (B) The illustration of a STAT3 inhibitor (SI109) docking with STAT3. The 3D illustration of lenticin and SI109 docking with the protein crystal of STAT3 (PDB ID: 6NJS) (Left pictures). The details of the lenticin and SI109 docking with the SH2 domain of STAT3 (amino acid residues from 584 to 688). The pink column-column represents H-bond and the orange column-circle represents the H- π bond (Middle pictures). The 2D diagrams of the top 5 components docking with STAT3 (Right pictures). (For interpretation of the references to color in this figure legend, the reader is referred to the Web version of this article.)

significantly increased in the UUO kidneys (Fig. 8B), which is abolished by treatment of both two doses of SSYR. These findings suggested that SSYR treatment attenuated pathological structures and suppressed tubulointerstitial fibrosis in UUO mice.

3.5. SSYR inhibited STAT3 activation in kidneys of UUO mice

The protein expression levels of phosphorylation of STAT3 and STAT3 were examined in kidney tissues (Fig. 9A). The expression of phospho-STAT3 (Tyr705) ($p < 0.01$; $p < 0.01$) and STAT3 ($p < 0.01$; $p < 0.01$) increased in the UUO group but dramatically suppressed in the 2.12 g/kg and 4.25 g/kg SSYR group (Fig. 9B).

4. Discussion

Although the etiology and pathological characteristics of renal fibrosis has been persistently investigated, there is no ideal drugs for preventing its progression and exhibiting no adverse side effects. TCM shows an extensive application potential in the prevention and treatment of renal fibrosis [12]. SSYR is prescribed base on traditional Chinese medicine theory and has been used in clinical practice for 30 years [13]. Since the complicated characteristics of traditional Chinese medicine, systematic network pharmacology was used to elucidate the specific mechanisms of SSYR underlying the renal fibrosis treatment.

UHPLC-Q-Orbitrap HRMS detection suggested that the main chemical components of 8 herbs in SSYR were flavonoids, organic acids, alkaloids, and anthraquinones, which may show a wide range of pharmacological activities with a variety of targets and pathways. Systematic network pharmacology indicated that the main active components belonged to Rhei Radix Et Rhizoma, Angelicae Sinensis Radix, and Astragali Radix. These 3 herbs were all essential and famous Chinese herbs used for thousands of years

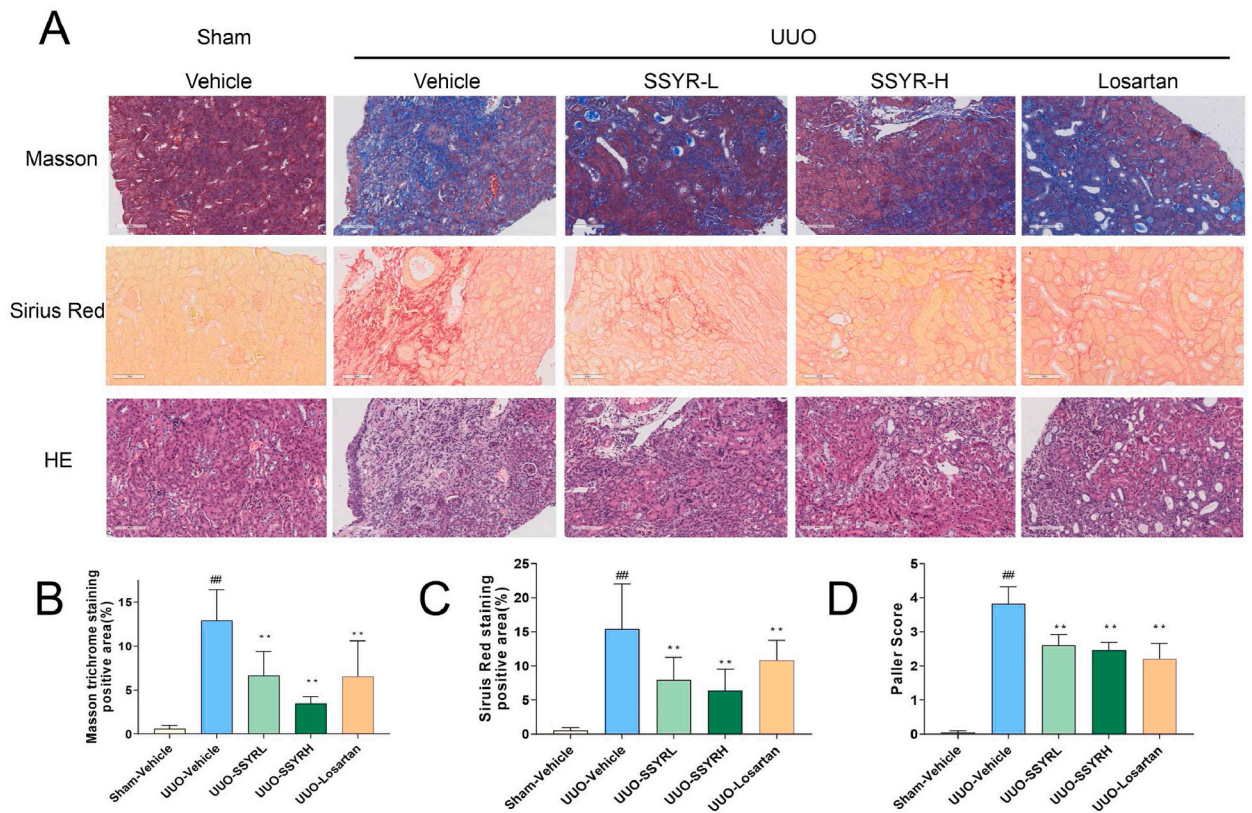


Fig. 7. SSYR alleviates kidney injury and renal fibrosis in the UUO model of CKD. (A) H&E staining of mouse tissue sections demonstrated degree of renal injury. Renal fibrosis was assessed by Masson's trichrome staining. Collagen deposition was measured by Sirius Red staining. (Magnification $\times 200$, Bar = 100 μm). (B) Semiquantitative result of renal fibrosis area (n = 7). (C) Tubular injury score of kidneys in the H&E staining. (D) Semiquantitative result of collagen deposition area (n = 7). Data represent mean \pm SD. $\#p < 0.05$ vs. sham-vehicle, $\#\#p < 0.01$ vs. sham-vehicle, $*p < 0.05$ vs. UUO-vehicle, $**p < 0.01$ vs. UUO-vehicle. (For interpretation of the references to color in this figure legend, the reader is referred to the Web version of this article.)

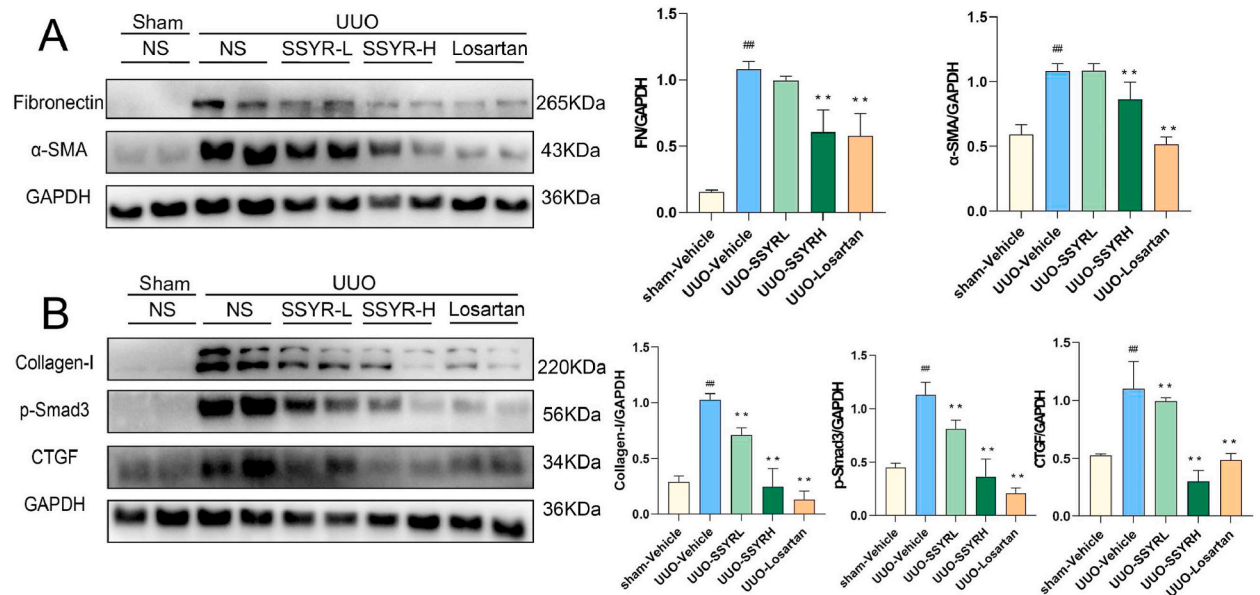


Fig. 8. SSYR alleviates pro-fibrotic proteins in the UUO model of CKD. (A) Immunoblot analysis of FN and α -SMA expression and relative quantitation in UUO kidneys. (B) Immunoblot analysis of Collagen-I, p-Smad3 and CTGF expression and relative quantitation in UUO kidneys. (n = 7). Data represent mean \pm SD. $\#p < 0.05$ vs. sham-vehicle, $\#\#p < 0.01$ vs. sham-vehicle, $*p < 0.05$ vs. UUO-vehicle, $**p < 0.01$ vs. UUO-vehicle.

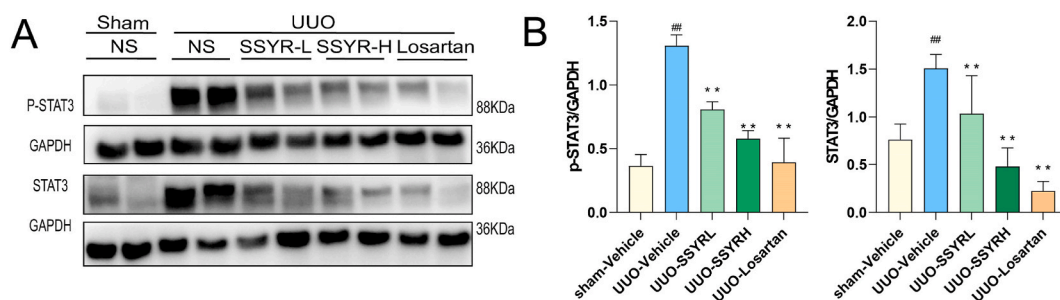


Fig. 9. SSYR inhibits renal fibrosis through inhibiting the expression of phospho-STAT3 (Tyr705) and STAT3 in obstructed kidneys. (A) Immunoblot analysis of phospho-STAT3 (Tyr705) and STAT3. (n = 7). #p < 0.05 vs. sham-vehicle, ##p < 0.01 vs. sham-vehicle, *p < 0.05 vs. UUO-vehicle, **p < 0.01 vs. UUO-vehicle.

[14]. They had very comprehensive pharmacological effects of anti-oxidation, anti-inflammation, and anti-fibroblast cells in several animal models and may be considered as the complementary therapeutic medicine for alleviating fibrosis [15–17].

In the current study, the chemical constituents screening and network pharmacological analysis gave a profile of pharmacodynamic material basis and systematic bioinformatic analysis showed the potent core targets of SSYR. STAT3 is a pleiotropic transcription factor activated by the phosphorylation of tyrosine 705 or the acetylation of Lys685 residues [18,19]. *In vivo*, STAT3 is the main driver of renal fibrosis through accumulating extracellular matrix [20], inducing multiple pro-fibrotic proteins and facilitating interstitial fibroblast proliferation [21,22]. *In vitro*, pharmacological inhibition or knock down of STAT3 activity attenuated the epithelial-mesenchymal transition of primary mouse renal tubular epithelial cells induced by TGF- β through inhibiting the phosphorylation of Smad3 and transcriptional activation of Snail [23]. Accordingly, STAT3 plays a critical role in the development of renal fibrosis [24].

Ureteral urinary obstruction in rodent can generate progressive renal fibrosis [25,26], which is characterized by tubular dilation, interstitial expansion, loss of proximal tubular mass, hydronephrosis, tubular epithelial cell death and presence of fibroblasts [27]. A dynamic model of UUO treated with SSYR in 13 days was taken to validate its mechanism of anti-fibrosis. SSYR significantly reduced the expressions of fibrotic markers and alleviated renal interstitial collagen deposition, which was potentially through blocking the phosphorylation of STAT3 and Smad3 and suppressing the expression of CTGF. So that the correlation between the protective effects of SSYR in renal fibrosis with the STAT3 phosphorylation signaling pathway was certified. To further prove our hypothesis that STAT3 mediates the protective effect of SSYR in renal fibrosis, some approaches to activation or inactivation of this signal pathway in the presence of SSYR should be taken in further work.

The results of virtual molecular docking revealed a component with a strong binding performance with potent target. Lenticin got a higher docking score than other constituents, which is the material basis for the core target in SSYR. Lenticin, also called hypaphorine, is an alkaloid from Vaccariae Semen, which is a member of the indole derivative family with pharmacological effect in anti-inflammation via NF- κ B and ERK pathways [28,29]. The mother structure of lenticin is close to the potent STAT3 inhibitor S1109 [30]. Their binding sites of STAT3 are very similar while they both bind solidly to the Ser613, Ser611, and Glu612 sites with H-bond in the pY pocket of SH2 domain which critically interferes with the phosphorylation of Tyr705 site. Furthermore, down-regulation of STAT3 phosphorylation would reduce inflammation levels and thus inhibiting fibrosis accumulation in the renal tissue or in fibroblasts induced by transforming growth factor (TGF- β) in TECs [31]. This evidence indicates that Lenticin may be a candidate active substance with inhibiting the phosphorylation of STAT3 in the anti-fibrosis properties of SSYR. Its inhibitory activity of STAT3 and anti-renal fibrosis effect will be further evaluated in the next work.

We also found several primary flavonoids, such as luteolin-7-O-rutinoside, kaempferol-3-O-rutinoside, and 3,5,6,7,8,3',4'-heptamethoxyflavone, showed comprehensive inhibitory activities of binding with STAT3, SRC, and Janus kinase 2 (JAK2) though their docking scores of STAT3 were not prominent. JAK2 and SRC are both up-streams of STAT3 [32,33]. By combining inhibiting the up-streams of STAT3 and directly blocking STAT3, these flavonoids may strengthen their inhibitory activities of STAT3 signaling pathway. As reported, luteolin-7-O-rutinoside could also reduce the release of IL-6, TNF- α , and IL-1 β and inhibit PI3K/AKT signaling pathway to attenuate acute liver injury [34]. Kaempferol-3-O-rutinoside inhibited the phosphorylation of STAT3 and the activation of NF- κ B to prevent ischemic brain injury and neuroinflammation. It also inhibited IL-6, TNF- α , and VEGF-C in LPS-induced RAW264.7 [35,36]. 3,5,6,7,8,3',4'-Heptamethoxyflavone suppressed IL-6, TNF- α , and IL-1 β in oxidized low-density lipoprotein-induced RAW264.7 macrophage-derived foam cell model [37]. Pro-inflammatory mediator IL-6 is also a crucial signal transducer which powerfully triggers the phosphorylation of JAK2/STAT3 signaling pathway [38]. These primary flavonoids may treat diseases via regulating the IL-6/STAT3 signaling pathway. In the further research, we will also evaluate the actual pharmacological effects and the regulation of IL-6/JAK2/STAT3 pathway of these three flavonoids in the treatment of RF *in vivo* and *in vitro*.

On the whole, SSYR could alleviate UUO-induced renal fibrosis, and STAT3 maybe the key therapeutic target of SSYR.

5. Conclusion

In this study, the active constituents and mechanisms of SSYR for treating RF were explored by integrating UHPLC-Q-Orbitrap HRMS, bioinformatics analysis and experimental pharmacology. Bioinformatics analysis suggested that STAT3 was the core target

and luteolin-7-O-rutinoside, hesperidin, kaempferol-3-O-rutinoside, and 3,5,6,7,8,3',4'-heptamethoxyflavone were the key constituents in SSYR for treating RF. SSYR alleviated renal fibrosis potentially blocked the phosphorylation of STAT3 and Smad3 and suppressed CTGF, suggesting that SSYR can be developed as a novel medicine for treating RF.

Ethics statement

The animal experiment was reviewed and approved by Committee on the Ethics of Animal Experiments of SHUTCM (Approval Number: PZSHUTCM220711030 and PZSHUTCM220711031). It was carried out in Experimental Animal Center of SHUTCM and conducted in accordance with the State Committee of Science and Technology of China.

Author contribution statement

Wei Liu: Conceived and designed the experiments; Analyzed and interpreted the data; Wrote the paper.

Jing Hu: Conceived and designed the experiments.

Tao-tao Weng, Lian-xiang Duan, Lin-zhang Zhang, Xia Wei, Sheng-lan Qi, Jia-wen You, Yu Cao, Yu Cao: Performed the experiments.

Guang-bo Ge: Analyzed and interpreted the data.

Pinglan Lin: Performed the experiments; Wrote the paper.

Xiao-li He: Conceived and designed the experiments; Wrote the paper.

Funding

This work was supported by the National Key Research and Development Program of China (No. 2021YFE0200900), National Natural Foundation of China (No. 82205009), 'Famous Traditional Chinese Medicine' Talent Training Plan of the Seventh People's Hospital affiliated to Shanghai University of Traditional Chinese Medicine (No. MZY2021-01), 'Medical Craftsman' Talent Training Plan of the Seventh People's Hospital affiliated to Shanghai University of Traditional Chinese Medicine, China (No. GJ2021-06), Pudong New Area Traditional Chinese Medicine Brand Multiplication Plan-Chronic Nephropathy (No. PDZY-2021-0302), 'Chen Guang' project supported by Shanghai Municipal Education Commission and Shanghai Education Development Foundation, China (No. 20CG50), Young Elite Scientists Sponsorship Program by CAST (No. 2020QNR001), Special Project for Clinical Research of Shanghai Municipal Health Commission (No. 20214Y0178), Budget Project of Shanghai University of Traditional Chinese Medicine (No. 2021LK092), Science Foundation of Yueyang Hospital of Integrated Traditional Chinese and Western Medicine (No. 2021yygq01).

Data availability statement

Data included in article/supp. material/referenced in article.

Declaration of competing interest

The authors declare that they have no known competing financial interests or personal relationships that could have appeared to influence the work reported in this paper.

Abbreviations

α -SMA	α -smooth muscle actin
CKD	chronic kidney disease
CTGF	connective tissue growth factor
ECM	extracellular matrix
FN	fibronectin
GO	Gene Ontology
HSP90AA1	heat shock protein 90AA1
IL-1 β	interleukin 1 β
IL-6	interleukin 6
JAK2	Janus kinase 2
MAPK3	mitogen-activated protein kinase 3
PTPN11	protein tyrosine phosphatase non receptor type 11
RF	renal fibrosis
R&S	renal fibrosis-related genes & SSYR potential targets
UHPLC-Q-Orbitrap HRMS	Ultra high performance liquid chromatography Q exactive hybrid quadrupole orbitrap high resolution accurate mass spectrometry
UUO	unilateral ureteral obstruction

STAT3	signal transducer and activator of transcription 3
SSYR	Shen-shuai-yi recipe
TCM	traditional Chinese medicine
TGF- β	transforming growth factor β
TICs	total ion chromatograms
TNF- α	tumor necrosis factor α

Appendix A. Supplementary data

Supplementary data to this article can be found online at <https://doi.org/10.1016/j.heliyon.2023.e17908>.

References

- [1] C. Yang, H.B. Wang, X.J. Zhao, K. Matsushita, J. Coresh, L.X. Zhang, et al., CKD in China: evolving spectrum and public health implications, *Am. J. Kidney Dis.* 76 (2020) 258–264, <https://doi.org/10.1053/j.ajkd.2019.05.032>.
- [2] L. Gewin, R. Zent, A. Pozzi, Progression of chronic kidney disease: too much cellular talk causes damage, *Kidney Int.* 91 (2017) 552–560, <https://doi.org/10.1016/j.kint.2016.08.025>.
- [3] A. Webster, E. Nagler, R. Morton, P. Masson, Chronic kidney disease, *Lancet* 389 (2017) 1238–1252, [https://doi.org/10.1016/S0140-6736\(16\)32064-5](https://doi.org/10.1016/S0140-6736(16)32064-5).
- [4] K.C. Huang, Y.C. Su, M.F. Sun, S.T. Huang, Chinese herbal medicine improves the long-term survival rate of patients with chronic kidney disease in Taiwan: a nationwide retrospective population-based cohort study, *Front. Pharmacol.* 9 (2018) 1117, <https://doi.org/10.3389/fphar.2018.01117>.
- [5] M.H. Shao, C.Y. Ye, G. Bayliss, S.G. Zhuang, New insights into the effects of individual Chinese herbal medicines on chronic kidney disease, *Front. Pharmacol.* 12 (2021), 774414, <https://doi.org/10.3389/fphar.2021.774414>.
- [6] B.B. Zhang, C.Y. Zhang, R.R. Pan, J. Chen, J.R. Lu, J.Y. Zhu, Optimization of the extraction technology of Shenshuaiyi decoction by comprehensive evaluation of multiple indexes, *Pharmaceut. Care Res.* 20 (2020) 23–27, <https://doi.org/10.5428/pcar20200106>.
- [7] H.Y. Han, J.R. Lu, X.H. Wang, Clinical effect of renal failure recipe on renal function and fibrosis in patients with early and middle-term chronic renal failure, *Chin. J. Exp. Trad. Med. Formul.* 22 (2016) 166–170, <https://doi.org/10.13422/j.cnki.syfjx.2016150166>.
- [8] J. Zou, X. Zhou, Y. Ma, R. Yu, Losartan ameliorates renal interstitial fibrosis through metabolic pathway and Smurfs-TGF- β /Smad, *Biomed. Pharmacother.* 149 (2022), 112931, <https://doi.org/10.1016/j.biopha.2022.112931>.
- [9] X.Q. Geng, A. Ma, J.Z. He, L. Wang, Y.L. Jia, G.Y. Shao, et al., Ganoderic acid hinders renal fibrosis via suppressing the TGF- β /Smad and MAPK signaling pathways, *Acta Pharmacol. Sin.* 41 (2020) 670–677, <https://doi.org/10.1038/s41401-019-0324-7>.
- [10] M. Paller, J. Hoidal, T. Ferris, Oxygen free radicals in ischemic acute renal failure in the rat, *J. Clin. Invest.* 74 (1984) 1156–1164, <https://doi.org/10.1172/JCI11524>.
- [11] P.L. Lin, F.R. Qiu, M. Wu, L. Xu, D. Huang, C. Wang, et al., Salvianolic acid B attenuates tubulointerstitial fibrosis by inhibiting EZH2 to regulate the PTEN/Akt pathway, *Pharm. Biol.* 61 (2022) 23–29, <https://doi.org/10.1080/13880209.2022.2148169>.
- [12] X.Y. Liu, X.B. Zhang, Y.F. Zhao, K. Qu, X.Y. Yu, Research progress of Chinese herbal medicine intervention in renal interstitial fibrosis, *Front. Pharmacol.* 13 (2022), 900491, <https://doi.org/10.3389/fphar.2022.900491>.
- [13] J. Chen, Y. Zheng, W.R. Liu, J.R. Lu, X.H. Wang, X.F. Chen, et al., Clinical effects and inflammation mechanism on renal failure with shenshuaiyi decoction, *J. Liaoning Univ. TCM* 18 (2016) 114–116, <https://doi.org/10.13194/j.issn.1673-842x.2016.09.034>.
- [14] L. Meng, V. Van Putten, L. Qu, R.A. Nemenoff, M.Y. Shang, S.Q. Cai, et al., Altered expression of genes profiles modulated by a combination of Astragali Radix and Angelicae Sinensis Radix in obstructed rat kidney, *Planta Med.* 76 (2010) 1431–1438, <https://doi.org/10.1055/s-0029-1240943>.
- [15] W.L. Wei, R. Zeng, C.M. Gu, Y. Qu, L.F. Huang, Angelica sinensis in China-A review of botanical profile, ethnopharmacology, phytochemistry and chemical analysis, *J. Ethnopharmacol.* 190 (2016) 116–141, <https://doi.org/10.1016/j.jep.2016.05.023>.
- [16] J. Fu, Z.H. Wang, L.F. Huang, S.H. Zheng, D.M. Wang, S.L. Chen, et al., Review of the botanical characteristics, phytochemistry, and pharmacology of Astragalus membranaceus (Huangqi), *Phytother. Res.* 28 (2014) 1275–1283, <https://doi.org/10.1002/ptr.5188>.
- [17] Y.L. Wang, Y. Feng, M.M. Li, M. Yang, G.X. Shi, Z.H. Xuan, et al., Traditional Chinese medicine in the treatment of chronic kidney diseases: theories, applications, and mechanisms, *Front. Pharmacol.* 13 (2022), 917975, <https://doi.org/10.3389/fphar.2022.917975>.
- [18] S.L. Zou, Q.Y. Tong, B.W. Liu, W. Huang, Y. Tian, X.H. Fu, Targeting STAT3 in cancer immunotherapy, *Mol. Cancer* 19 (2020) 145, <https://doi.org/10.1186/s12943-020-01258-7>.
- [19] E.J. Hillmer, H. Zhang, H.S. Li, S.S. Watowich, STAT3 signaling in immunity, *Cytokine Growth Factor Rev.* 31 (2016) 1–15, <https://doi.org/10.1016/j.cytogr.2016.05.001>.
- [20] M.Y. Pang, L. Ma, R.J. Gong, E. Tolbert, H.P. Mao, M. Ponnusamy, et al., A novel STAT3 inhibitor, S3I-201, attenuates renal interstitial fibroblast activation and interstitial fibrosis in obstructive nephropathy, *Kidney Int.* 78 (2010) 257–268, <https://doi.org/10.1038/ki.2010.154>.
- [21] W. Chen, H. Yuan, W.M. Cao, T.W. Wang, W. Chen, H. Yu, et al., Blocking interleukin-6 trans-signaling protects against renal fibrosis by suppressing STAT3 activation, *Theranostics* 9 (2019) 3980–3991, <https://doi.org/10.7150/thno.32352>.
- [22] J. Ni, Y. Shen, Z. Wang, D.C. Shao, J. Liu, L.J. Fu, et al., Inhibition of STAT3 acetylation is associated with angiotensin renal fibrosis in the obstructed kidney, *Acta Pharmacol. Sin.* 35 (2014) 1045–1054, <https://doi.org/10.1038/aps.2014.42>.
- [23] J.S. Liu, Y. Zhong, G.Y. Liu, X.B. Zhang, B.F. Xiao, S. Huang, et al., Role of Stat3 signaling in control of EMT of tubular epithelial cells during renal fibrosis, *Cell. Physiol. Biochem.* 42 (2017) 2552–2558, <https://doi.org/10.1159/000480216>.
- [24] P.Y. Chuang, J.C. He, JAK/STAT signaling in renal diseases, *Kidney Int.* 78 (2010) 231–234, <https://doi.org/10.1038/ki.2010.158>.
- [25] R.L. Chevalier, M.S. Forbes, B.A. Thornhill, Ureteral obstruction as a model of renal interstitial fibrosis and obstructive nephropathy, *Kidney Int.* 75 (2009) 1145–1152, <https://doi.org/10.1038/ki.2009.86>.
- [26] X.X. Zhou, X.J. Zang, M. Ponnusamy, Enhancer of zeste homolog 2 inhibition attenuates renal fibrosis by maintaining Smad7 and phosphatase and tensin homolog expression, *J. Am. Soc. Nephrol.* 27 (2016) 2092–2108, <https://doi.org/10.1681/ASN.2015040457>.
- [27] E. Martínez-Klimova, O.E. Aparicio-Trejo, E. Tapia, Unilateral ureteral obstruction as a model to investigate fibrosis-attenuating treatments, *Biomolecules* 9 (2019) 141, <https://doi.org/10.3390/biom9040141>.
- [28] M. Ozawa, K. Honda, I. Nakai, A. Kishida, A. Ohsaki, Hypaphorine, an indole alkaloid from *Erythrina velutina*, induced sleep on normal mice, *Bioorg. Med. Chem. Lett.* 18 (2008) 3992–3994, <https://doi.org/10.1016/j.bmcl.2008.06.002>.
- [29] H.J. Sun, W.W. Cai, X. Wang, Y.L. Liu, B. Hou, X.X. Zhu, et al., Vaccaria hypaphorine alleviates lipopolysaccharide-induced inflammation via inactivation of NF- κ B and ERK pathways in Raw 264.7 cells, *BMC Compl. Altern. Med.* 17 (2017) 120, <https://doi.org/10.1186/s12906-017-1635-1>.
- [30] H.B. Zhou, L.C. Bai, R.Q. Xu, Y.J. Zhao, J.Y. Chen, D. McEachern, et al., Structure-Based discovery of SD-36 as a potent, selective, and efficacious PROTAC degrader of STAT3 protein, *J. Med. Chem.* 62 (2019) 11280–11300, <https://doi.org/10.1021/acs.jmedchem.9b01530>.
- [31] Y. Bai, W. Wang, P. Yin, J. Gao, L. Na, Y. Sun, et al., Ruxolitinib alleviates renal interstitial fibrosis in UUO mice, *Int. J. Biol. Sci.* 16 (2020) 194–203, <https://doi.org/10.7150/ijbs.39024>.

- [32] K.T. Yuan, J.N. Ye, Z.G. Liu, Y. F Ren, W.L. He, J.B. Xu, et al., Complement C3 overexpression activates JAK2/STAT3 pathway and correlates with gastric cancer progression, *J. Exp. Clin. Cancer Res.* 39 (2020) 9, <https://doi.org/10.1186/s13046-019-1514-3>.
- [33] Y.X. Liu, B.W. Xu, X.D. Niu, Y.J. Chen, X.Q. Fu, X.Q. Wang, et al., Inhibition of Src/STAT3 signaling-mediated angiogenesis is involved in the anti-melanoma effects of dioscin, *Pharmacol. Res.* 175 (2022), 105983, <https://doi.org/10.1016/j.phrs.2021.105983>.
- [34] Z.W. Xiong, Y.S. Cui, J. H Wu, L.Y. Shi, W. Quan, S.L. Yang, et al., Luteolin-7-O-rutinoside from *Pteris cretica* L. var. *nervosa* attenuates LPS/D-gal-induced acute liver injury by inhibiting PI3K/AKT/AMPK/NF- κ B signaling pathway, *Naunyn-Schmiedeberg's Arch. Pharmacol.* 395 (2022) 1283–1295, <https://doi.org/10.1007/s00210-022-02266-8>.
- [35] L. Yu, C. Chen, L.F. Wang, X. Kuang, K. Liu, H. Zhang, et al., Neuroprotective effect of kaempferol glycosides against brain injury and neuroinflammation by inhibiting the activation of NF- κ B and STAT3 in transient focal stroke, *PLoS One* 8 (2013), e55839, <https://doi.org/10.1371/journal.pone.0055839>.
- [36] W.H. Hu, D.K. Dai, B.Z. Zheng, R. Duan, G.K. Chan, T.T. Dong, et al., The binding of kaempferol-3-O-rutinoside to vascular endothelial growth factor potentiates anti-inflammatory efficiencies in lipopolysaccharide-treated mouse macrophage RAW264.7 cells, *Phytomedicine* 80 (2021), 153400, <https://doi.org/10.1016/j.phymed.2020.153400>.
- [37] P.L. Liang, Q.W. Liang, P.W. He, X.L. Chen, Y. Xu, H.S. Tu, et al., Three polymethoxyflavones from the peel of *Citrus reticulata* 'Chachi' inhibits oxidized low-density lipoprotein-induced macrophage-derived foam cell formation, *Front. Cardiovasc. Med.* 9 (2022), 924551, <https://doi.org/10.3389/fcvm.2022.924551>.
- [38] D.E. Johnson, R.A. O'Keefe, J.R. Grandis, Targeting the IL-6/JAK/STAT3 signaling axis in cancer, *Nat. Rev. Clin. Oncol.* 15 (2018) 234–248, <https://doi.org/10.1038/nrclinonc.2018.8>.